AAAS
Research
Volume 2020, Article ID 2640834, 11 pages
https://doi.org/10.34133/2020/2640834

Research Article

The Possibility of Changing the Wettability of Material Surface by Adjusting Gravity

Yong-Ming Liu,[1,2] **Zi-Qing Wu**,[1] **Sheng Bao**,[1] **Wei-Hong Guo**,[1] **Da-Wei Li**,[1] **Jin He**,[1] **Xiang-Bin Zeng**,[1] **Lin-Jun Huang**,[1] **Qin-Qin Lu**,[1] **Yun-Zhu Guo**,[1] **Rui-Qing Chen**,[1] **Ya-Jing Ye**,[1] **Chen-Yan Zhang**,[1] **Xu-Dong Deng**,[1] **and Da-Chuan Yin**[1,3]

[1]*Key Lab of Space Bioscience & Biotechnology, School of Life Sciences, Northwestern Polytechnical University, Xi'an, 710072 Shaanxi, China*
[2]*School of Bioengineering, Sichuan University of Science and Engineering, Zigong, 643000 Sichuan, China*
[3]*Shenzhen Research Institute of Northwestern Polytechnical University, Shenzhen, 518057 Guangdong, China*

Correspondence should be addressed to Da-Chuan Yin; yindc@nwpu.edu.cn

Received 7 July 2019; Accepted 1 January 2020; Published 27 January 2020

The contact angle, as a vital measured parameter of wettability of material surface, has long been in dispute whether it is affected by gravity. Herein, we measured the advancing and receding contact angles on extremely low contact angle hysteresis surfaces under different gravities (1-8G) and found that both of them decrease with the increase of the gravity. The underlying mechanism is revealed to be the contact angle hysteresis and the deformation of the liquid-vapor interface away from the solid surface caused by gradient distribution of the hydrostatic pressure. The real contact angle is not affected by gravity and cannot measured by an optical method. The measured apparent contact angles are angles of inclination of the liquid-vapor interface away from the solid surface. Furthermore, a new equation is proposed based on the balance of forces acting on the three-phase contact region, which quantitatively reveals the relation of the apparent contact angle with the interfacial tensions and gravity. This finding can provide new horizons for solving the debate on whether gravity affects the contact angle and may be useful for the accurate measurement of the contact angle and the development of a new contact angle measurement system.

1. Introduction

Wetting is one of the basic characteristics of solid surfaces. It is very important for processes like adhesion [1], self-cleaning [2], fluid drag reduction [3], heterogeneous nucleation [4], and the formation of coffee rings [5]. Therefore, it has attracted immense interest in a large diversity of research fields ranging from physical, biological, and environmental sciences. Owing to its complexity, wetting and the parameter used to measure it, the contact angle, have been investigated for many years [6–27]. Currently, thousands of papers are published annually about the topic. However, there are still fundamental questions to be answered. The relationship between the wetting and gravity is one of them.

In 1805, Young pointed out that every solid-liquid pair has an "appropriate angle of contact" [6]. This "appropriate angle of contact" is called Young's contact angle. According to his description, a famous equation named Young's equation can be written as

$$\gamma_{lv} \cos \theta_Y = \gamma_{sv} - \gamma_{sl}, \tag{1}$$

where γ_{lv} is the liquid-vapor interfacial tension, γ_{sv} is the solid-vapor interfacial tension, γ_{sl} is the solid-liquid interfacial tension, and θ_Y is Young's contact angle for a drop on a solid.

Because the disjoining pressure, resulted from the intermolecular interaction, makes the structure of three-phase contact line complicated, Benner et al. [28] referred to Young's equation not being valid, and the alternative equations for contact angle were derived by other researchers [29–32] based on various intermolecular force models. This issue was resolved by Keller and Merchant [33], and a precise

mathematical definition for the contact angle was proposed: a boundary condition to the Young-Laplace equation where the film thickness is 0. Physically, as addressed by de Gennes [34], Young's contact angle is a measurable macroscopic contact angle which is on a scale above that of long-ranged intermolecular forces [34]. At present, it is considered that Young's equation describes the relationship between macroscopic, measurable, thermodynamic variables, and the contact angle. And the interfacial tensions refer to the constant, interfacial Gibbs free energies far from the contact line. In Young's equation, gravity is not included as a variable.

Some researchers [8–14] also derived the same Young's equation based on the thermodynamics of wetting and pointed out that the contact angle depends only on the physical and chemical properties of the solid, liquid, and vapor accordingly and is not affected by gravity. Gravity only affects the shape of the drop [8–14]. Recently, Bormashenko imposing the transversality conditions on the variational problem of wetting also demonstrates that gravity does not influence equilibrium contact angles [35–37]. However, many experimental observations [15–27] under some gravities (≤2G) differed from these theoretical conclusions. This discrepancy becomes an important issue, especially in the space era, when interfacial phenomena frequently draw more attention because they are dominant events in microgravity and much different from those observed on Earth. Extensive studies on wetting and the contact angle are beneficial for clarifying this issue.

It is generally believed that Young's contact angle represents the contact angle of the liquid on an ideal surface, which refers to a rigid, smooth, chemically homogeneous, and inert surface. On an ideal surface, the system has a single and unique contact angle. However, for a real solid surface and a liquid, many contact angles can be measured since the system has many metastable equilibrium states, and each metastable equilibrium state corresponds to one contact angle [38]. Among these contact angles, the lowest metastable contact angle is the receding contact angle, and the highest one is the advancing contact angle [38]. They can be measured by receding and advancing liquid on a solid surface [7, 38, 39]. And the difference between advancing and receding contact angles is called contact angle hysteresis. Nearly all real solid surfaces exhibit contact angle hysteresis [7, 39, 40]. Only a few smooth, chemically homogeneous, and inert real surfaces possess very low contact angle hysteresis [41, 42]. They are the ones that most closely approach an ideal surface. The contact angles on these low contact angle hysteresis surfaces are very close to Young's contact angle. Previous experimental studies [15–27, 43] at different gravities used ordinary surfaces. Thus, the results of the effect of gravity on the contact angle may be caused by contact angle hysteresis. To rule out this possibility, it is necessary to systematically study the relationship between the contact angle and gravity using surfaces with low contact angle hysteresis.

In addition to the requirement for using low contact angle hysteresis surfaces, clarification of the relationship between the contact angle and gravity needs to consider the drop size.

Even on ideal surfaces, the contact angle is affected by the drop volume increases, due to line tension σ [9, 44]. Equation (2) is the line tension-modified Young's equation:

$$\gamma_{sv} = \gamma_{lv} \cdot \cos\theta_Y + \gamma_{sl} + \frac{\sigma}{R}, \tag{2}$$

where R is the three-phase contact radius.

According to Equation (2), when the drop is large enough, the effect of the line tension σ can be ignored [7, 38]. Furthermore, in order for the measurement and interpretation to be meaningful, the drop must be sufficiently large compared with the size scale of heterogeneity that ensures the drop base is axisymmetric [45]. Therefore, reproducible and reliable measurement of the contact angle shall be carried out using large drops. In the literatures, it has been reported that the radius of the sessile drop should be larger than 2.5-3.5 mm [46] or even larger than 3.0-5.0 mm [7], especially for chemically and morphologically heterogeneous surfaces. In previous experimental measurements of the contact angle under different gravities, large drops were rarely used.

In general, the sessile droplet on an inclined plate (real surface, not idea surface) will be deformed due to the pinning of the contact line and gravity, and the contact angle will be changed by gravity [47–51]. This issue was widely investigated by researchers [47–51]. The tilt plate method is also used to measure the advancing and receding contact angle. However, they are related to the weight of the drop. According to literature report, the advancing and receding contact angles obtained by the tilt plate method are not consistent with that obtained by the sessile drop [38, 45]. Thus, the sessile drop method is employed in this study.

In this study, the advancing and receding contact angles of large drops on solid surfaces with extremely low contact angle hysteresis under a wide range of gravities (1-8 G) were measured for the first time. The large range of hypergravities (1-8 G) were generated by a long-arm ($d = 6$ m) centrifuge which was specially designed and developed for the accurate measurement of apparent contact angles via a remote control. The dynamic process of gravity affecting the apparent contact angle was analyzed by solving the augmented Young-Laplace equation. The relationship between the contact angle measured by the optical method and the real contact angle was discussed. And a new equation describing the relationship between gravity and the apparent contact angle was presented. The discovery can provide new horizons for solving the debate on whether gravity affects contact angle and may be useful for the accurate measurement of the contact angle and the development of a new contact angle measurement system.

2. Results

2.1. Long-Arm Centrifuge and Contact Angle Measurement Unit. The contact angles of liquids on solid surfaces were measured under different gravities generated by a homemade specially designed long-arm ($d = 6$ m) centrifuge (Figures 1(a) and 1(b)). The maximum rotation rate of this centrifuge is 65 RPM. It can provide a stable and long durable

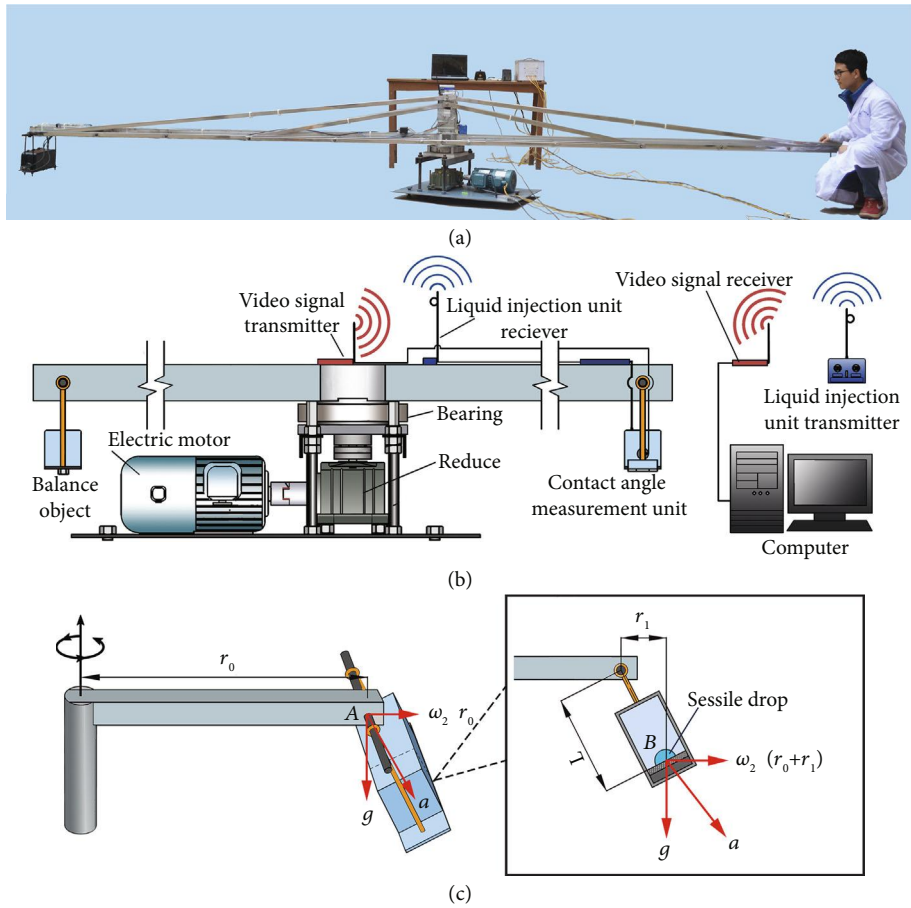

FIGURE 1: Long-arm centrifuge and contact angle measurement unit. (a) Photograph of the long-arm centrifuge and contact angle measurement unit. (b) Diagram of the long-arm centrifuge and contact angle measurement unit. (c) Diagram of centrifugation force. In a gravitational field, the acceleration of an object with the vector sum of the centrifugal and gravity forces at point A is $\sqrt{g^2 + (\omega^2 r_0)^2}$, and at point B, it is $\sqrt{g^2 + [\omega^2(r_0 + r_1)]^2}$. Owing to $L << r_0$, $\sqrt{g^2 + [\omega^2(r_0 + r_1)]^2} \approx \sqrt{g^2 + (\omega^2 r_0)^2}$. The centrifugal acceleration gradient of the centrifuge is ~0.0028 G/mm.

gravity level of 1-8 G. The contact between the liquid and solid surface takes place at point B which is inside a sealed box in the contact angle measurement unit (Figure 1(c)). The contact angle measurement unit (Figure 1) hangs on one end of the long-arm, while an object of the same weight hangs on the other end of the long-arm for balance (Figure 1(b)). The liquid can be injected onto or withdrawn from the solid surface through a syringe via a remote liquid control unit (Figure 1(b)). A CCD camera equipped with a low distortion telecentric lens (resolution: 22~37 lp/mm) is used to capture the contact process between the liquid and solid surface, and a video of this process can be transmitted by a wireless video transmission system (Figure 1(b)). From the video, the images of the sessile drops can be captured, and the contact angle can be determined from the images using the DropSnake program [52].

2.2. Contact Angles at Different Gravities. In this work, silicon wafers were treated using DMDCS (dimethyldichlorosilane), PDMS^{2K} (trimethylsilyl-terminated linear poly (dimethylsiloxane), MW 2,000), and PDMS^{9K} (trimethylsilyl-terminated linear poly (dimethylsiloxane), MW 9,000) to obtain smooth surfaces with low contact angle hysteresis. Their morphologies were studied by AFM (Atomic Force Microscope) (Figure 2(a)). It can be seen that the roughness of all surfaces is ~1 nm. Compared with the DMDCS, PDMS^{2K} and PDMS^{9K} have many small hills, and those of the PDMS^{9K} are rougher than those of the PDMS^{2K}. The low-rate dynamic contact angles of water, ethylene glycol, and glycerol on these surfaces were measured under 1-8 G. Figure S1 shows the measurement results of the contact angle of water on DMDCS at different gravities. The results show that the DMDCS was indeed low contact angle hysteresis surface. Most of the other surfaces also exhibited the same properties. Figure 2(b) shows the contact angles of different liquids on different solid surfaces at 1-8 G. It can be seen that the contact angle hysteresis was very low (<3°) in most cases except for ethylene glycol and glycerol on PDMS^{9K}. Generally, surface roughness and chemical heterogeneity will lead to pinning of the three-phase contact line, which subsequently results in contact angle hysteresis [35, 53]. For the PDMS^{9K}, the pinning effect of these small hills on the

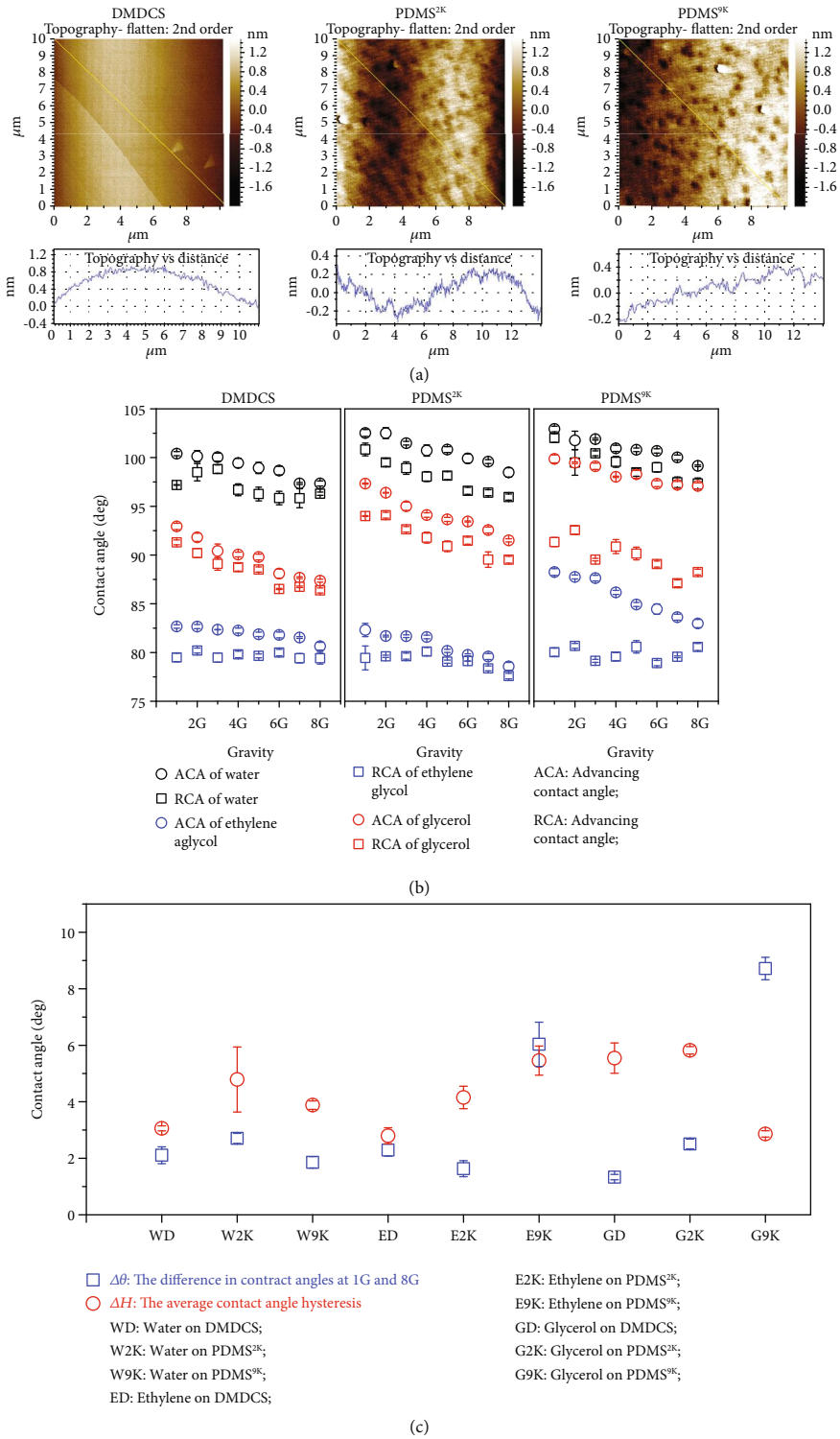

FIGURE 2: Apparent contact angles versus gravity. (a) AFM images of the sample solid surfaces and their section analyses. The analyses show that the surfaces are very smooth, with roughness less than 1 nm. (b) The contact angle on solid surfaces at different gravities. The contact angles show the same tendency to decrease with increasing gravity. The contact angle hysteresis was smaller than 3°, except for the cases of ethylene glycol and glycerol on PDMS^{9K}. (c) Comparison of $\Delta\theta$ (the difference in contract angles at 1 G and 8 G) and ΔH (the average contact angle hysteresis). Independent t-test was applied, $n = 3$, $P < 0.05$, $P < 0.001$, $P < 0.001$, $P < 0.05$, $P < 0.001$, and $P < 0.001$, for water on DMDCS, water on PDMS^{9K}, ethylene glycol on PDMS^{2K}, glycerol on DMDCS, glycerol on PDMS^{2K}, and glycerol on PDMS^{9K}, respectively. Five out of the nine solid-liquid contact systems showed significant larger $\Delta\theta$ than ΔH, three showed comparable results. The experimental results confirmed that the decrease in the contact angle upon increasing gravity is caused by gravity, not only by the contact angle hysteresis.

three-phase contact line may be the reason for the relatively larger contact angle hysteresis.

From Figure 2(b), it can also be seen that the apparent contact angle decreased as gravity increased, especially for the advancing contact angle. Although low contact angle hysteresis surfaces were used in this study, the contact angle hysteresis still exists. Thus, the decrease of the apparent contact angle with the increase of gravity may be related to contact angle hysteresis.

For a drop on a real surface, the wetting state is generally in a metastable equilibrium state, and the most stable equilibrium state is difficult to achieve because many energy barriers need to be overcome [38]. The advancing and receding contact angles can be easily measured because of the low energy barrier [38]. Generally, additional energy can overcome the energy barrier and make the wetting state reach a more stable equilibrium state [38, 45]. The direct result is that the additional energy decreases the advancing contact angle and increases the receding contact angle [38]. The increasing gravity may provide additional energy to make wetting reach a more stable state, so that the advancing and receding contact angles are different under different gravities. However, upon checking the data in Figure 2(b) more carefully, we found that all receding contact angles do not increase with the increase of gravity as predicted by theory except receding contact angles of ethylene glycol on DMDCS and PDMS^{9K}. In addition, by comparing $\Delta\theta$ (the difference in the contact angles at 1 G and 8 G) and ΔH (the average contact angle hysteresis) (Figure 2(c)), we also found that in six of nine liquid-solid contact systems, $\Delta\theta$ was greater than ΔH. This means that the apparent contact angle decrease relative to the increasing gravity was not only caused by contact angle hysteresis.

2.3. Hydrostatic Pressure at Different Gravities. As showed in Figures 2(b) and 2(c), the apparent contact angles are affected by gravity. The direct consequence of gravity for a drop is the presence of the hydrostatic pressure, which means that the apparent contact angle under gravity is related to the hydrostatic pressure.

Figure 3(a) shows example images of the sessile drop (water on DMDCS, $R = 2.5$ mm) under gravities ranging from 1 to 8 G. It can be seen that the height h of the drops decreased upon increasing gravity (Figure 3(b)). However, the hydrostatic pressure ρgh at the three-phase contact line was increasing during the increase of gravity g (Figure 3(c)). This result means that the effect of gravity on the hydrostatic pressure is more significant than that of the drop height. The results of all hydrostatic pressure cases investigated in this research are summarized in Figure 3(d), which show that the hydrostatic pressure does increase with increasing gravity, despite the height of the drop decreasing with increasing gravity. However, how does the hydrostatic pressure affects the apparent contact angle?

In the conventional analysis of the equilibrium of forces near the three-phase contact line, Young's equation was obtained [6] (Figure 3(e)), and the hydrostatic pressure was not considered. In gravitational field, the diagram of the hydrostatic pressure (red arrows) acting on the liquid-vapor interface of the drop of the three-phase contact region is shown in Figure 3(f). The hydrostatic pressure increases from 0 to ρgh from the top to the bottom of the drop. As shown in Figure 3(f), the drop will be deformed due to the hydrostatic pressure, leading to a smaller contact angle as compared with that without considering gravity. With increasing gravity, the hydrostatic pressure will increase, so that the deformation of the drop will be more significant, resulting in a smaller contact angle (Figure 3(d)).

However, theoretically, the contact angle has nothing to do with gravity, whether the disjoining pressure is ignored (such as derivation of Young's equation by Bormashenko [35, 36]) or considered (for an example, the classical work by Starov and Velarde [37]). This is in contradiction with our experimental results. The possible reason is that the contact angles we measured are the apparent contact angles, not the mathematically defined contact angles. They are on the liquid-vapor interface and away from the solid surface due to the low resolution of the measurement system. If the resolution of the measurement system is high enough, we will see the real three-phase contact region. In this region, viscous resistance, resulted from the intermolecular interaction, is very high. Compared with the disjoining pressure, ~10^6 N/m^2, the hydrostatic pressure (~10^2 N/m^2 under 8G) is much smaller, and it is impossible to deform the liquid-vapor interface in the three-phase contact region. The deformation of liquid-vapor interface caused by hydrostatic pressure can only occur in the area controlled by capillary action far away from the solid surface and the three-phase contact region. The situation shown in Figure 3(d) is just a macrosituation. In fact, the measured apparent contact angles are the angles of inclination of a certain position on the liquid-vapor interface. In order to confirm this point, it is necessary to study the relationship between droplet profile and inclination angle under different gravities.

2.4. Drop Profile, Angle of Inclination of Liquid-Vapor Interface, and Contact Angle under Different Gravities. In this part, we use the method of Diaz et al. [31] to deduce the relationship between drop profile and inclination angle of liquid-vapor interface. Figure 4 shows the 2D profile of a liquid-vapor interface shape in the vicinity of the contact line. As shown in Figure 4, there are three regions—molecular, transition, and capillary regions. The molecular region is dominated by the disjoining pressure and spatially varying interfacial free energies resulted from the molecular interaction; the capillary region is dominated by the capillarity and gravity; and in the transition region, the disjoining pressure competes with the hydrostatic pressure, and the surface tension is assumed constant. Within the molecular region, the equation for the shape of the liquid-vapor interface is the fully augmented Young-Laplace equation [31]:

$$g_{\mathrm{lv}}(h,\theta)2H = -\prod(h,\theta) - (p_l - p_v), \tag{3}$$

where $g_{\mathrm{lv}}(h,\theta)$ is liquid-vapor interfacial free energy, h is the film thickness, θ is the angle of inclination of the liquid-vapor interface, $2H$ is the curvature, $\Pi(h,\theta)$ is the disjoining

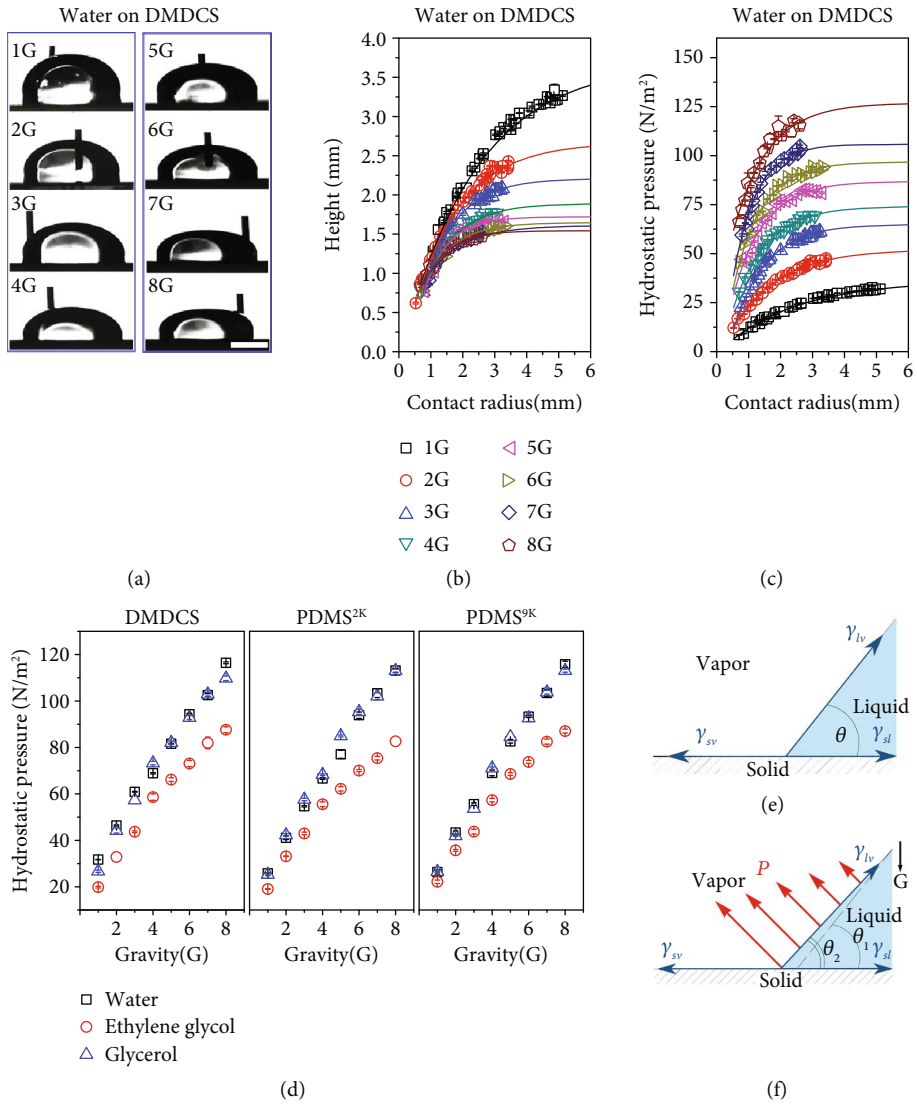

FIGURE 3: Hydrostatic pressure at different gravities. (a) Sessile water drop on DMDCS at different gravities ($R = 2.5$ mm). At higher gravity, the drop deforms and its height decreases more obviously. (b) Height versus the three-phase contact radius for sessile water drops on DMDCS surface under 1-8 G gravity. (c) Hydrostatic pressure at the three-phase contact line versus the three-phase contact radius for sessile water drops on a DMDCS surface under 1-8 G gravity. (d) Hydrostatic pressure at the three-phase contact line versus the different gravities. (e) Conventional analysis of the equilibrium of forces near the three-phase contact line (gravity is not considered). (f) Equilibrium of forces near the three-phase contact line of a sessile drop (gravity is considered). The experimental measurement shows that although the height decreases, the hydrostatic pressure increases monotonously with gravity, indicating that hydrostatic pressure should not be neglected, especially when gravity is large. The qualitative analysis in (f) shows that gravity can decrease the contact angle.

pressure, p_l is the pressure in liquid, and p_v is the pressure in vapor. Above the molecular region, $g_{lv}(h, \theta)$ becomes a constant, γ_{lv}.

In Equation (3), $2H$ can be expressed by

$$2H = -\frac{d \cos \theta}{dh}. \tag{4}$$

For convenience, considering only the contribution from Van der Waals force, the disjoining pressure can be expressed by

$$-\prod(h, \theta) = \frac{A_{LL} G(\theta) - A_{SL}}{6\pi h^3}, \tag{5}$$

where A is Hamaker constants, $G(\theta) = (1/2) + (3/4) \cos \theta - (1/4) \cos^3 \theta$ [54].

By introducing a molecular film thickness, h_m,

$$h_m = \frac{A_{LL} G(\theta_0) - A_{SL}}{6\pi \gamma_{lv}}, \tag{6}$$

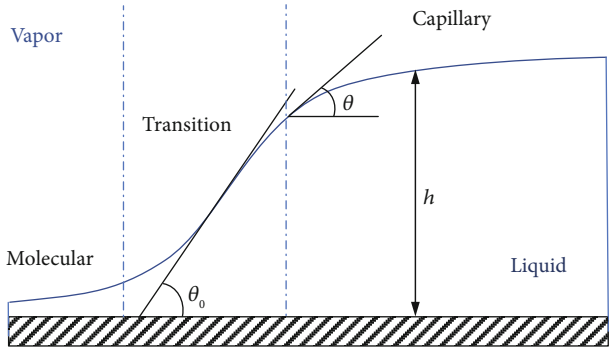

Figure 4: Interface shape in the vicinity of the contact line. There are three regions: capillary region, molecular region, and transition region. θ: angle of inclination of liquid-vapor interface; θ_0: contact angle, where the surface forces are neglected and $h = 0$.

then,

$$\prod(h) = -\gamma_{lv}\frac{h_m^2}{h^3}. \tag{7}$$

For the liquid slice, the hydrostatic pressure at any point on the interface can be expressed by

$$p_l - p_v = \rho g(h_e - h), \tag{8}$$

where h_e, the equilibrium height of the drop, is a certain constant at a particular gravitational level; h is the height of any point on the liquid-vapor interface.

Outside the molecular region, an augmented Young-Laplace equation can be obtained by combining Equations (3), (4), (7), and (8)

$$-\frac{d\cos\theta}{dh} = \frac{h_m^2}{h^3} - \frac{h_e - h}{(\kappa^{-1})^2}, \tag{9}$$

where $\kappa^{-1} = \sqrt{\gamma_{lv}/\rho g}$ is the capillary length.

Integrating Equation (9) and imposing $h = h_e, \theta = 0$ yields the solution

$$\cos\theta = \frac{h_m^2}{2h^2} - \frac{h_m^2}{2h_e} + 1 - \frac{h_e^2}{2\cdot(\kappa^{-1})^2} + \frac{hh_e}{(\kappa^{-1})^2} - \frac{h^2}{2\cdot(\kappa^{-1})^2}. \tag{10}$$

Without the disjoining pressure, Equation (10) becomes the Young-Laplace equation:

$$\cos\theta = 1 - \frac{h_e^2}{2\cdot(\kappa^{-1})^2} + \frac{hh_e}{(\kappa^{-1})^2} - \frac{h^2}{2\cdot(\kappa^{-1})^2}. \tag{11}$$

Figure 5(a) shows a variation of the angle θ of the water drop on DMDCS with the film thickness h under different gravity (θ is calculated by using Equation (10) and assuming $h_m = 2\times10^{-9}$ m). It can be seen that the transition region, where the film curvature is negligible, decreases with the increasing gravity. When gravity increases to 100,000 G, the linear transition region of the liquid-vapor interface begins to deform. However, the contact angle θ_0 ($h = 0$ m) is independent of gravity. Only above the transition region, the angles of inclination of the liquid-vapor interface decrease with the increase of gravity.

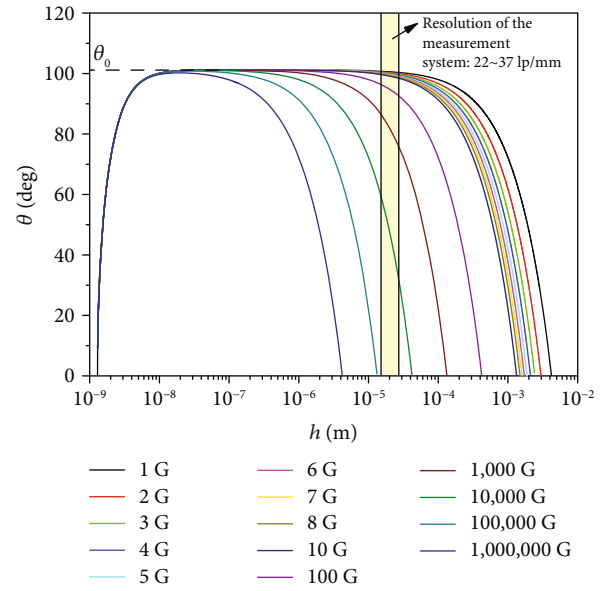

Figure 5: Variation of the water contact angle θ on DMDCS with the film thickness h under different gravities. The dashed line is the solution of the Young-Laplace equation (Equation (11)); the colored line is the solution of the augmented Young-Laplace equation (Equation (10)).

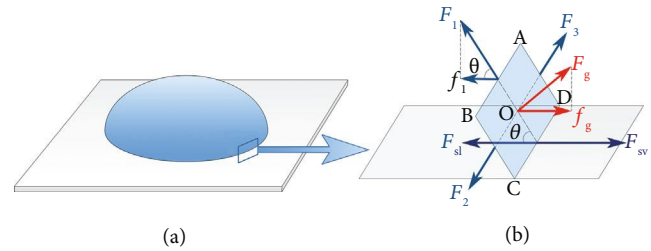

Figure 6: Equilibrium of forces near the three-phase contact line of sessile drop. (a) Diagram of a sessile drop. (b) Equilibrium of forces near the three-phase contact line. F_{sl} and F_{sv}: solid-liquid and the solid-vapor interfacial tension forces; F_g and f_g: force caused by the hydrostatic pressure and its horizontal component; F_1, F_2, and F_3: liquid-vapor interfacial tension forces; f_1: horizontal component of F_1; θ: the apparent contact angle.

In this study, the resolution of the measurement system is of 22~37 lp/mm. That is, the minimum size that the measurement system can identify is of 2.7×10^{-5}~4.5×10^{-5} m. On this scale, our experimental results (Figure 2(b)) are in good agreement with the theoretical values (Figure 5). That means the measured apparent contact angles, θ_{ma}, are angles of inclination of the liquid-vapor interface at a distance of 10^{-4}~10^{-5} m from the solid surface. In other words, the

Table 1: h_s values (μm) of the solid-liquid contact system.

Gravity	Water on DMDCS	Ethylene glycol on DMDCS	Glycerol on DMDCS	Water on PDMS^{2k}	Ethylene glycol on PDMS^{2k}	Glycerol on PDMS^{2k}	Water on PDMS^{9k}	Ethylene glycol on PDMS^{9k}	Glycerol on PDMS^{9k}
1 G	22.6	13.3	13.2	22.2	18.2	12.9	9.5	29.0	4.8
2 G	22.6	12.5	30.4	19.4	23.7	26.3	30.8	28.9	4.8
3 G	20.4	12.5	46.5	29.5	19.7	42.4	22.6	25.0	4.8
4 G	25.3	11.6	45.6	22.6	17.7	49.1	32.9	39.7	6.6
5 G	32.2	14.1	45.2	31.8	30.6	49.2	31.9	48.6	8.6
6 G	30.2	13.2	57.9	38.9	31.8	47.2	30.0	50.1	23.2
7 G	40.3	14.9	57.8	39.7	30.8	52.1	35.0	52.1	22.8
8 G	38.2	21.3	56.8	48.2	37.4	58.4	41.1	54.1	22.7
Average	28.9 ± 2.7	14.2 ± 1.1	44.2 ± 5.5	31.5 ± 3.6	26.2 ± 2.6	42.2 ± 5.3	29.2 ± 3.4	40.9 ± 4.2	12.3 ± 3.1

measured apparent contact angles are not the real contact angles. The measured apparent contact angles depend on the resolution of the measurement system.

From Figure 5, we can also see that the lower the gravity is, or the higher the resolution of measurement system is, the closer the measured apparent contact angle is to the real contact angle. Therefore, it is suggested to measure the contact angle under a lower gravity environment or using a higher resolution measurement system.

In this section, for convenience, only the distribution of Van der Waals force to the disjoining pressure was considered. In fact, for water, other two components, electrostatic component and structural component, are also important components for the disjoining pressure. Unfortunately, there are no firm and precise theoretical equations for these two components [55]. The real shape of the three-phase contact region for water or aqueous solution under high gravity may be very complex.

2.5. Relationship between Apparent Contact Angle and Gravity. The contact angle is independent on gravity. However, the measured apparent contact angle, which is an angle of inclination of the liquid-vapor interface away from the solid surface, can be affected by gravity. It is related to the resolution of the measurement system. In order to clarify the relationship between the apparent contact angle and gravity, neglecting completely the disjoining pressure, we used the mechanical method of deriving the Young-Laplace equation [56], with consideration of the presence of hydrostatic pressure, liquid-vapor, solid-vapor, and solid-liquid interfacial tensions. And for this large drop, we consider a small rectangular section (ABCD, Figure 6) of the liquid-vapor interface at the three-phase contact line, where CD is a segment of the apparent three-phase contact line. The liquid-vapor interfacial tension forces pull the three edges of surface ABCD along the tangent direction perpendicular to the edges, and the solid-liquid and the solid-vapor interfacial tension forces F_{sl} and F_{sv} pull the side of CD along the horizontal direction. If the sessile drop is in gravity g, the surface ABCD will experience a hydrostatic pressure, resulting in a force F_g that is perpendicular to the surface. The sum of the forces in the horizontal direction must be zero (detail showed in Supplementary Materials). And a new equation can be written as below:

$$\gamma_{sv} = \gamma_{lv} \cdot \cos\theta + \gamma_{sl} - \rho g h_e h_s, \tag{12}$$

where h_e is the height of the drop and h_s,$BC \cdot \sin\theta$, is an unknown length and is related to the resolution of the measurement system. When h_s equals to 0, the measured apparent contact angle will be equal to the real contact angle. When h_s is not equal to 0, the apparent contact angle is dependent on gravity g. The larger the h_s is, the more obvious is the influence of gravity on the contact angle.

From Equation (12), it can be seen that the dependence of the apparent contact angle on gravity depends on h_s. Therefore, it is possible to use the calculated contact angle to fit the measured apparent contact angle by adjusting the value of the length h_s. The schematic flowchart of the calculation process is shown in Figure S2. Table 1 shows the results of the value of h_s. From Table 1, we can see that the scale of the h_s value is 10^{-4}~10^{-5} m. It is also consistent with the results which are shown in Figure 5 and the resolution of measurement system which is used in this study.

3. Discussion

In this work, we found that the contact angle was not affected by gravity, while the measured apparent contact angle was gravity-dependent. The measured apparent contact angle is not the real contact angle. Actually, it is the angle of inclination of the liquid-vapor interface far away from the solid surface. The contact angle cannot be measured by the optical method because it depends on the resolution of the measurement system. However, using a high-solution measurement system, one can obtained an approximation of the contact angle. This is of great significance for the accurate measurement of the contact angle and the development of a new contact angle measurement system. Furthermore, with the combination of theoretical derivation and experimental measurements, we obtained a new equation (Equation (12)), which can be used to calculate the apparent contact angle at different gravities based on the resolution of measurement

system. This study can provide new horizons for solving the debate on whether gravity affects contact angle.

4. Materials and Methods

Purified water (18 MΩ·cm, obtained using a Millipore Milli-Q system), ethylene glycol (CP, purchased from Sinopharm Chemical Reagent Co. Ltd., China), and glycerol (CP, purchased from Sinopharm Chemical Reagent Co. Ltd., China) were chosen as probe liquids.

Silicon wafers (100 orientation, P/B doped, resistivity from 20 to 40 Ω·cm) were chosen as the substrate for the preparation of the probe surface, which were purchased from Zhejiang Li Jing Silicon Material Co. Ltd., China. Disks (4 inches) was cut into rectangular shapes of about 2 cm × 4 cm and then soaked in a freshly prepared mixture of 7 parts concentrated with sulfuric acid and 3 parts 30% hydrogen peroxide at 150°C for 30 min, rinsed with purified water, dried in a clean oven at 120°C for 1-2 h, and then allowed to cool to room temperature.

4.1. Preparation of DMDCS Surface. The dry silicon wafers were transferred to a flask containing 0.5 mL of DMDCS. To make sure there was no direct contact between the liquids and solid surfaces, silicon wafers were placed in an oven at 70°C for 3 days, and then rinsed sequentially with toluene, ethanol, ethanol-purified water (1 : 1), and purified water, and dried in a clean oven at 120°C for 1-2 h [42].

4.2. Preparation of PDMS Surface. The dry silicon wafers were transferred to a flask and wet with $PDMS^{2K}$ or $PDMS^{9K}$(purchased from Sinopharm Chemical Reagent Co. Ltd., China), placed in a clean oven at 100°C for 24 h, rinsed sequentially by copious toluene, acetone, and purified water, and dried in a clean oven at 120°C for 1-2 h [41].

4.3. Determination of Solid Surface Morphology. The surface morphology was studied using atomic force microscopy (PicoPlus AFM, manufactured by Modular Imaging, USA), and tapping mode was selected. The scanned domain was 10.0 μm × 10.0 μm. The roughness of the sample surfaces was analyzed from the AFM images with PicoView 1.12 Software (Agilent Technologies, USA).

4.4. Measurement of Contact Angle. The contact angles of liquids on solid surfaces were measured under different gravities generated by a long-arm centrifuge. Each measurement was carried out at a new location on the sample surface. The advancing/receding velocity of the three-phase contact line was 0.1-1.5 mm/min.

Data Availability

All data are available in the manuscript or supplementary materials.

Conflicts of Interest

The authors declare that there is no conflict of interest regarding the publication of this article.

Authors' Contributions

Y. M. Liu designed the experimental apparatuses, performed all of the experiments, analyzed the data, did theoretical analyses, and prepared the manuscript. D. C. Yin designed and supervised this study, did theoretical analyses, and revised the manuscript. Z. Q. Wu designed and manufactured the centrifuge and assisted in all of the experiments. S. Bao, W. H. Guo, D. W. Li, X. B. Zeng, L. J. Huang, and J. He performed the surface treatment of samples. Q. Q. Lu, C. Y. Zhang, X. D. Deng, Y. J. Ye, Y. Z. Guo, and R. Q. Chen analyzed the source data. Y. M. Liu and Z. Q. Wu contributed equally.

Acknowledgments

This work was supported by the National Natural Science Foundation of China (Grant No. U1632126), and the Scientific Research Foundation for the Introduction of Talent of Sichuan University of Science and Engineering (Grant No. 2017RCL75).

Supplementary Materials

Figure S1: variation of the contact angle with the three-phase contact radius under different gravities. (a)–(h) The contact angles versus time for water on a DMDCS surface under 1-8 G gravitational levels. (a′)– (h′) The three-phase contact radius versus time under 1-8 G gravity. Figure S2: schematic flowchart for calculation. (a) Schematic flowchart for adjusting the value of the length h_s. (b) Young's contact angles (θ_Y), solid surface tensions (γ_{sv}), and solid-liquid interfacial tensions (γ_{sl}) of solid-liquid contact systems. (c) The maximum height of the large sessile drop at equilibrium under different gravities. (2) Derivation of the relationship between gravity and the apparent contact angle. (3) Calculation of the value of the solid-liquid interfacial tension and solid surface tension. *(Supplementary Materials)*

References

[1] Y. Sun and Z. Guo, "Recent advances of bioinspired functional materials with specific wettability: from nature and beyond nature," *Nanoscale Horizons*, vol. 4, no. 1, pp. 52–76, 2019.

[2] K. Liu, M. Vuckovac, M. Latikka, T. Huhtamäki, and R. H. A. Ras, "Improving surface-wetting characterization," *Science*, vol. 363, no. 6432, pp. 1147-1148, 2019.

[3] H. Geng, H. Bai, Y. Fan et al., "Unidirectional water delivery on a superhydrophilic surface with two-dimensional asymmetrical wettability barriers," *Materials Horizons*, vol. 5, no. 2, pp. 303–308, 2018.

[4] X. Yao, S. Wu, L. Chen et al., "Self-replenishable anti-waxing organogel materials," *Angewandte Chemie, International Edition*, vol. 54, no. 31, pp. 8975–8979, 2015.

[5] M. Anyfantakis and D. Baigl, "Dynamic photocontrol of the coffee-ring effect with optically tunable particle stickiness," *Angewandte Chemie, International Edition*, vol. 126, no. 51, pp. 14301–14305, 2014.

[6] T. Young, "III. An essay on the cohesion of fluids," *Philosophical Transactions of the Royal Society of London*, vol. 95, pp. 65–87, 1805.

[7] D. Y. Kwok and A. W. Neumann, "Contact angle measurement and contact angle interpretation," *Advances in Colloid and Interface Science*, vol. 81, no. 3, pp. 167–249, 1999.

[8] J. E. Mcnutt and G. M. Andes, "Relationship of the contact angle to interfacial energies," *The Journal of Chemical Physics*, vol. 30, no. 5, pp. 1300–1303, 1959.

[9] R. J. Good and M. N. Koo, "The effect of drop size on contact angle," *Journal of Colloid and Interface Science*, vol. 71, no. 2, pp. 283–292, 1979.

[10] K. Jakhar, A. Chattopadhyay, A. Thakur, and R. Raj, "Spline based shape prediction and analysis of uniformly rotating sessile and pendant droplets," *Langmuir*, vol. 33, no. 22, pp. 5603–5612, 2017.

[11] E. M. Blokhuis, Y. Shilkrot, and B. Widom, "Young's law with gravity," *Molecular Physics*, vol. 86, no. 4, pp. 891–899, 1995.

[12] Y. Larher, "A very simple derivation of Young's law with gravity using a cylindrical meniscus," *Langmuir*, vol. 13, no. 26, pp. 7299-7300, 1997.

[13] J. P. Garandet, B. Drevet, and N. Eustathopoulos, "On the validity of Young's equation in the presence of gravitational and other external force fields," *Scripta Materialia*, vol. 38, no. 9, pp. 1391–1397, 1998.

[14] P. Roura and J. Fort, "Local thermodynamic derivation of Young's equation," *Journal of Colloid and Interface Science*, vol. 272, no. 2, pp. 420–429, 2004.

[15] H. Sakai and T. Fujii, "The dependence of the apparent contact angles on gravity," *Journal of Colloid and Interface Science*, vol. 210, no. 1, pp. 152–156, 1999.

[16] L. Hong, H. Zhang, X. Luo, B. Ding, Z. Mai, and Z. Hu, "Effect of gravity on wettability and interface between liquid AG-CU-SN alloy and solid iron substrate," in *34th COSPAR Scientific Assembly, The Second World Space Congress*, Houston, TX, USA., October, 2002.

[17] A. Ababneh, A. Amirfazli, and J. A. W. Elliott, "Effect of gravity on the macroscopic advancing contact angle of sessile drops," *The Canadian Journal of Chemical Engineering*, vol. 84, no. 1, pp. 39–43, 2006.

[18] D. Brutin, Z. Q. Zhu, O. Rahli, J. C. Xie, Q. S. Liu, and L. Tadrist, "Sessile drop in microgravity: creation, contact angle and interface," *Microgravity Science and Technology*, vol. 21, no. S1, pp. 67–76, 2009.

[19] Z. Q. Zhu, D. Brutin, Q. S. Liu et al., "Experimental investigation of pendant and sessile drops in microgravity," *Microgravity Science and Technology*, vol. 22, no. 3, pp. 339–345, 2010.

[20] M. V. Bartashevich, V. V. Kuznetsov, and O. A. Kabov, "Gravity effect on the axisymmetric drop spreading," *Microgravity Science and Technology*, vol. 22, no. 1, pp. 107–114, 2010.

[21] T. Enz, S. Steinbach, D. Simicic, G. Kasperovich, and L. Ratke, "First experiments using the materials science laboratory on board the international space station," *Microgravity Science and Technology*, vol. 23, no. 3, pp. 345–353, 2011.

[22] A. Diana, M. Castillo, D. Brutin, and T. Steinberg, "Sessile drop wettability in normal and reduced gravity," *Microgravity Science and Technology*, vol. 24, no. 3, pp. 195–202, 2012.

[23] Z. Q. Zhu, Y. Wang, Q. S. Liu, and J. C. Xie, "Influence of bond number on behaviors of liquid drops deposited onto solid substrates," *Microgravity Science and Technology*, vol. 24, no. 3, pp. 181–188, 2012.

[24] Y. M. Liu, R. Q. Chen, Z. Q. Wu et al., "Measurement of contact angles in a simulated microgravity environment generated by a large gradient magnetic field," *The Review of Scientific Instruments*, vol. 87, no. 9, p. 095107, 2016.

[25] Y. V. Naidich, I. I. Gab, T. V. Stetsyuk, and B. D. Kostyuk, "Simulation of the microgravity effect on wettability of solids with different liquids," *Powder Metallurgy and Metal Ceramics*, vol. 55, no. 11-12, pp. 726–731, 2017.

[26] A. Calvimontes, "The measurement of the surface energy of solids by sessile drop accelerometry," *Microgravity Science and Technology*, vol. 30, no. 3, pp. 277–293, 2018.

[27] A. Calvimontes, *Young's equation vs. sessile drop accelerometry: a comparison using the interfacial energies of seven polymer-water systems*, vol. 3, Reprints, 2018.

[28] R. E. Benner, L. E. Scriven, and H. T. Davis, "Structure and stress in the gas–liquid–solid contact region," *Faraday Symposia of the Chemical Society*, vol. 16, pp. 169–190, 1981.

[29] M. V. Berry, "Simple fluids near rigid solids: statistical mechanics of density and contact angle," *Journal of Physics A: Mathematical, Nuclear and General*, vol. 7, no. 2, pp. 231–245, 1974.

[30] G. J. Jameson and M. C. G. del Cerro, "Theory for the equilibrium contact angle between a gas, a liquid and a solid," *Journal of the Chemical Society, Faraday Transactions 1: Physical Chemistry in Condensed Phases*, vol. 72, pp. 883–895, 1976.

[31] M. E. Diaz, J. Fuentes, R. L. Cerro, and M. D. Savage, "An analytical solution for a partially wetting puddle and the location of the static contact angle," *Journal of Colloid and Interface Science*, vol. 348, no. 1, pp. 232–239, 2010.

[32] M. E. Diaz, M. D. Savage, and R. L. Cerro, "Prediction of static contact angles on the basis of molecular forces and adsorption data," *Physical Review E*, vol. 94, no. 2, 2016.

[33] J. B. Keller and G. J. Merchant, "Flexural rigidity of a liquid surface," *Journal of Statistical Physics*, vol. 63, no. 5-6, pp. 1039–1051, 1991.

[34] P. G. de Gennes, "Wetting: statics and dynamics," *Reviews of Modern Physics*, vol. 57, no. 3, pp. 827–863, 1985.

[35] E. Bormashenko, "Young, Boruvka-Neumann, Wenzel and Cassie-Baxter equations as the transversality conditions for the variational problem of wetting," *Colloids and Surfaces A: Physicochemical and Engineering Aspects*, vol. 345, no. 1-3, pp. 163–165, 2009.

[36] E. Bormashenko, "Variational framework for defining contact angles: a general thermodynamic approach," *Journal of Adhesion Science and Technology*, vol. 34, no. 2, pp. 219–230, 2020.

[37] V. M. Starov and M. G. Velarde, "Surface forces and wetting phenomena," *Journal of Physics: Condensed Matter*, vol. 21, no. 46, p. 464121, 2009.

[38] A. Marmur, "Solid-surface characterization by wetting," *Annual Review of Materials Research*, vol. 39, no. 1, pp. 473–489, 2009.

[39] H. Y. Erbil, "The debate on the dependence of apparent contact angles on drop contact area or three-phase contact line: a review," *Surface Science Reports*, vol. 69, no. 4, pp. 325–365, 2014.

[40] L. Gao and T. J. Mccarthy, "Wetting 101°†," *Langmuir*, vol. 25, no. 24, pp. 14105–14115, 2009.

[41] L. Wang and T. J. Mccarthy, "Covalently attached liquids: instant omniphobic surfaces with unprecedented repellency," *Angewandte Chemie, International Edition*, vol. 128, no. 1, pp. 252–256, 2016.

[42] A. Y. Fadeev and T. J. McCarthy, "Self-assembly is not the only reaction possible between alkyltrichlorosilanes and surfaces: monomolecular and oligomeric covalently attached layers of dichloro- and trichloroalkylsilanes on silicon," *Langmuir*, vol. 16, no. 18, pp. 7268–7274, 2000.

[43] S. Gulec, S. Yadav, R. Das, V. Bhave, and R. Tadmor, "The influence of gravity on contact angle and circumference of sessile and pendant drops has a crucial historic aspect," *Langmuir*, vol. 35, no. 16, pp. 5435–5441, 2019.

[44] J. K. Berg, C. M. Weber, and H. Riegler, "Impact of negative line tension on the shape of nanometer-size sessile droplets," *Physical Review Letters*, vol. 105, no. 7, p. 076103, 2010.

[45] T. Huhtamäki, X. Tian, J. T. Korhonen, and R. H. A. Ras, "Surface-wetting characterization using contact-angle measurements," *Nature Protocols*, vol. 13, no. 7, pp. 1521–1538, 2018.

[46] J. Drelich, "Guidelines to measurements of reproducible contact angles using a sessile-drop technique," *Surface Innovations*, vol. 1, no. 4, pp. 248–254, 2013.

[47] R. Goodwin, D. Rice, and S. Middleman, "A model for the onset of motion of a sessile liquid drop on a rotating disk," *Journal of Colloid and Interface Science*, vol. 125, no. 1, pp. 162–169, 1988.

[48] E. B. Dussan V and R. T.-P. Chow, "On the ability of drops or bubbles to stick to non-horizontal surfaces of solids," *Journal of Fluid Mechanics*, vol. 137, pp. 1–29, 1983.

[49] S. Padmanabhan and A. Bose, "On the anomalous behavior of surfactant contaminated drops," *Journal of Colloid and Interface Science*, vol. 139, no. 2, pp. 535–540, 1990.

[50] A. I. ElSherbini and A. M. Jacobi, "Retention forces and contact angles for critical liquid drops on non- horizontal surfaces," *Journal of Colloid and Interface Science*, vol. 299, no. 2, pp. 841–849, 2006.

[51] R. Tadmor, P. Bahadur, A. Leh, H. E. N'guessan, R. Jaini, and L. Dang, "Measurement of lateral adhesion forces at the interface between a liquid drop and a substrate," *Physical Review Letters*, vol. 103, no. 26, p. 266101, 2009.

[52] A. F. Stalder, G. Kulik, D. Sage, L. Barbieri, and P. Hoffmann, "A snake-based approach to accurate determination of both contact points and contact angles," *Colloids and Surfaces A: Physicochemical and Engineering Aspects*, vol. 286, no. 1-3, pp. 92–103, 2006.

[53] H. Perrin, R. Lhermerout, K. Davitt, E. Rolley, and B. Andreotti, "Defects at the nanoscale impact contact line motion at all scales," *Physical Review Letters*, vol. 116, no. 18, p. 184502, 2016.

[54] J. Fuentes, "Dynamics of moving, three-phase contact lines," *PhD Thesis, Chemical and Materials Engineering*, University of Alabama in Huntsville, 2003.

[55] V. M. Starov and M. G. Velarde, *Wetting and spreading dynamics*, CRC Press, Boca Raton, 2019.

[56] S. Vafaei and D. Wen, "Modification of the Young-Laplace equation and prediction of bubble interface in the presence of nanoparticles," *Advances in Colloid and Interface Science*, vol. 225, pp. 1–15, 2015.